Received: Added at production | Revised: Added at production | Accepted: Added at production

DOI: xxx/xxxx

ARTICLE TYPE

A combined polar and Cartesian piecewise trajectory generation and analysis of a robotic arm

Mihai Dupac*

[1]Org Division, Org name, State name, Country name
[2]Org Division, Org name, State name, Country name
[3]Org Division, Org name, State name, Country name

Correspondence
*Mihai Dupac, Bournemouth University, UK. mdupac@bournemouth.ac.uk

Present Address
Present address

Summary

In this paper a combined polar-Cartesian approach to generate a smooth trajectory of a robotic arm along priori defined via-points is presented. Due to the characteristics/-geometry of the robotic arm, cylindrical coordinates are associated with the trajectory of motion. Possible trajectories representing the system dynamics are generated by mix matching higher order polar piecewise polynomials used to devise the radial trajectory and Cartesian piecewise polynomials used to calculate the related height in a normal plane unfolded along the radial trajectory of the motion. To describe the kinematic properties of the end-effector a moving non-inertial orthonormal Frenet frame is considered. Using the Frenet frame, the components of the velocity and acceleration along the frame unit vectors are calculated. Numerical simulations are performed for two different configurations in order to validate the approach.

KEYWORDS:
Path planning, piecewise interpolation, kinematics, dynamics

1 | INTRODUCTION

Trajectory planning of robotic manipulators is considered a fundamental factor in industry and automation with important consequences in improving production life cycle and minimizing costs [1]. The capacity to plan smooth trajectories involve taking into consideration kinematic constraints [2,3], execution time [4] and jerk [5].

The last decade have seen important research into the assessment of novel lightweight robotic devices specifically designed for rehabilitation [6]. This include a novel system [7] to measure and analyse the kinetic data as a way to develop and improve robotic rehabilitation systems. An adaptive trajectory generation approach for a bilateral upper arm rehabilitation training have been considered in [8], and a novel filtered kinematic matrix adaptive control was examined in [9]. A robotic platform for upper arm neuro-rehabilitation was considered in [10]. In [11] the movements of a human arm are considered and analysed in order to describe the kinematic of an upper arm exoskeleton rehabilitation robot with two actuators. The kinematics and dynamics of a Pantograph based rehabilitation robot is considered in [12] as a way to create a robust control that allow stroke patients [10] to complete rehabilitation exercises of their upper arm, elbow or shoulder.

Piecewise interpolating functions with high continuity and/or geometrically continuous splines [13,14,15] are adequate tools in generating smooth motion of the robotic manipulators when the manipulator kinematics (velocity, acceleration [16] and/or jerk) or dynamics (force and/or torque) is considered [17]. Such approach [13] should reduce resonant frequency excitation and generate smoother trajectory profile. The interpolation of smooth curves (twice-differentiable and cubic in the parametrized co-ordinates) invariant with respect to the fixed/moving frame represent an excellent approach to minimize angular acceleration [16]. A new planning approach of an manipulator along a set of nodal points for a collection of established kinematical requirements is presented in[18]. Kinematic variables and joint-space trajectories can be easily calculated/planned through a sequence of specified joints for smooth and continuous motion while preserving the C^k continuity[19].

In this study the modelling and simulation of 3D smooth trajectories of a related robotic arm using piecewise interpolants is addressed. Path planning of the robotic arm is devised using a given number of via-points the end-effector should reach. Due to the geometry constraints, i.e., a trajectory does not exist outside the working envelope, the relation between the geometry of the robotic arm and its base location is examined. Possible trajectories are generated using Hermite polar piecewise interpolants for the projected radial trajectory on the Oxy plane combined with a linear approximation of the trajectory height. Two sets of numerical results to highlight the correlation between the geometry and the working envelope are presented.

2 | MANIPULATOR MODEL AND TRAJECTORY GENERATION

The robotic arm is represented by a z-guide (link 0) denoted by zG, a rigid sliding guide (link 1) denoted by RG and a sliding link (link 2) denoted by SL as shown in Fig. 1.a. The z-guide (link 0) of the robotic arm represented in a fixed Cartesian reference frame $Oxyz$ can rotate about the Oz axis. The rigid guide (link 1) of the robotic arm can slide up and down on the z-guide (link 0) to reach a desired height while rotating (with the z-guide) about the Oz axis. Link 2 and the rigid guide are joined by the means of a slider joint, that is, the link can slide in and out of the rigid guide[20,21] as shown in Fig. 1.a. The length of the z-guide is l_z, the length of the rigid guide is l_{RG} and the length of the sliding link is l_{SL}.

The interpolated trajectory T_{P_i} along the via-points $P_i, i = \overline{1, n}$ (Fig. 1).a is represented using

$$\mathbf{r}_{P_{i_k}} = r_{P_{i_k}} \cos\theta_{P_{i_k}} \mathbf{i}_0 + r_{P_{i_k}} \sin\theta_{P_{i_k}} \mathbf{j}_0 + z_{P_{i_k}} \mathbf{k}_0 \tag{1}$$

where T_{P_i} represents the 3 dimensional piecewise trajectory followed by the end-effector, P_{i_k} represents the interpolating points along the pricewise curve defined by the via-points P_i and P_{i+1}, $r_{P_{i_k}} = d\left(O_1, P_{i_k}\right)$ is the radial distance/radius from the point O_1 (of the mobile reference frame $O_1x_1y_1z_1$ attached to the rigid guide (link 1)) to the point P_{i_k}, $z_{P_{i_k}}$ is the associated height (distance from P_{i_k} to $O_0x_0y_0$), and $\theta_{P_{i_k}}$ is the azimuthal coordinate given in an anticlockwise direction. When the end-effector describes the 3 dimensional piecewise trajectory T_{P_i} given by the via-points $P_i, i = \overline{1, n}$, its projection on the $O_0x_0y_0$ plane is the planar polar trajectory described by $Q_i\left(r_{P_{i_k}} \cos\theta_{P_{i_k}}, r_{P_{i_k}} \sin\theta_{P_{i_k}}\right)$.

To interpolate between the via-points $P_i, i = \overline{0, N_i}$ specified by the data $\left\{r_i, \theta_i, z_i\right\}_{i=\overline{0,N_i}}$ (Fig. 1.a), the combination between a piecewise polar interpolation (that approximate the projected radial interpolation shown in Fig. 1.c) and a Cartesian interpolation (Fig. 1.b) was considered. For each interval $\left[\theta_i, \theta_{i+1}\right]_{i=\overline{0,N_i-1}}$ and lengths r_i and r_{i+1} of the consecutive points Q_i and Q_{i+1}, a polar piecewise interpolantion (Fig. 1.c) can be devised as a Hermite-type polinomial[22,23,24,25]

$$r(\theta) = \sum_{k=0}^{q} c_k^i \left(\theta - \theta_i\right)^k \tag{2}$$

where $c_0^i = r_i$, $c_1^i = \dot{r}_i$, $c_2^i = \frac{1}{h_i}\left[\left(2\dot{r}_i + \dot{r}_{i+1}\right) + 3\Delta r_i\right]$, $c_3^i = \frac{1}{h_i^2}\left[\dot{r}_i + \dot{r}_{i+1} - 2\Delta r_i\right]$, $r_i = r\left(\theta_i\right)$, $r_{i+1} = r\left(\theta_{i+1}\right)$, $h_i = \theta_{i+1} - \theta_i$, $\Delta y_i = \frac{r_{i+1} - r_i}{h_i}$, $\dot{r}\left(\theta_i\right) = \frac{dr(\theta_i)}{d\theta} = \dot{r}_i$ and $\dot{r}\left(\theta_{i+1}\right) = \frac{dr(\theta_{i+1})}{d\theta} = \dot{r}_{i+1}$.

Trajectory height, which relates the change in height with the piecewise polar trajectory of motion (Fig. 1.b), is computed in the unfolded normal plane ((Fig. 1.a)) tracking the radial trajectory (Fig. 1.c). The computation is performed by Cartesian piecewise interpolation with Hermite polynomials[22,23,24,25] defined by

$$z(x) = \sum_{k=0}^{q} C_k^i \left(x - x_i\right)^k \tag{3}$$

where q is the order of the polynomial, $h_i = x_{i+1} - x_i$, $z_i = z\left(x_i\right)$, $z_{i+1} = z\left(z_{i+1}\right)$, $\Delta z_i = \frac{z_{i+1} - z_i}{h_i}$ $C_0^i = z_i$, $C_1^i = \dot{z}_i$, $C_2^i = \frac{1}{h_i}\left[\left(2\dot{z}_i + \dot{z}_{i+1}\right) + 3\Delta z_i\right]$, $C_3^i = \frac{1}{h_i^2}\left[\dot{z}_i + \dot{z}_{i+1} - 2\Delta z_i\right]$, and where the derivatives at the endpoints P_i and P_{i+1} are calculated as $\dot{z}\left(x_i\right) = \frac{dz(x_i)}{dx} = \dot{z}_i$ and $\dot{z}\left(x_{i+1}\right) = \frac{dz(x_{i+1})}{dx} = \dot{z}_{i+1}$ respectively.

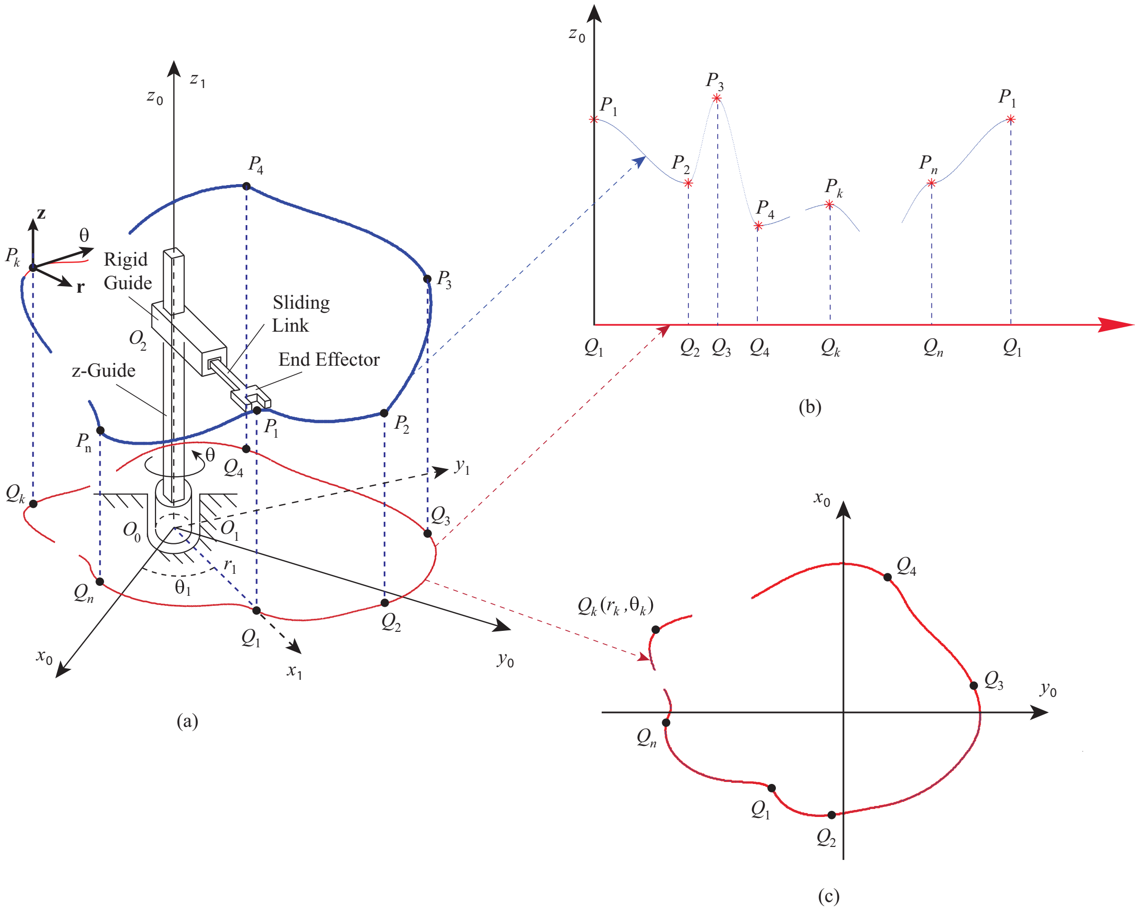

FIGURE 1 (a) Rotating extensible robotic arm model, (b–c) Trajectory of the end-effector $r(\theta)$ expressed as a combination of polar and Cartesian Hermite-type function

The variable x in Eq.(3) is the length of the curve shown in Fig. 1.c and represents the polar trajectory of motion. The length of the trajectory shown in Fig. 1.c through the points Q_i and Q_{i+1} is calculated using

$$l\left(Q_i, Q_{i+1}\right) = \int_{\theta_i}^{\theta_{i+1}} \sqrt{r^2 + \left(\frac{dr}{d\theta}\right)^2} d\theta \tag{4}$$

where $r = r(\theta)$ is given by Eq.2. The distance $d\left(O, P_{i_k}\right)$ is calculated using

$$d\left(O, P_{i_k}\right) = \sqrt{r_{i_k}^2 + z_{i_k}^2} dx \tag{5}$$

where z_{i_k} is the height of each trajectory point, r_{i_k} is given by Eq.1, and the maximal and minimal distance from the robotic arm base to the end-effector trajectory T_{P_i}, is calculated as in[24] using

$$d_{min} = \inf_{P_{i_k} \in T_{P_i}} d\left(O, P_{i_k}\right), \quad d_{max} = \sup_{P_{i_k} \in T_{P_i}} d\left(O, P_{i_k}\right) \tag{6}$$

Since the geometric path T_{P_i} of the robotic arm should be reachable by the end-effector, i.e., the trajectory does not exist outside the envelope of the robotic arm, the length/geometry of the extensible arm conveys the existence of a solution. That is, a trajectory exists if and only if the system

$$\begin{cases} r_{max} & \leq l_{LG} + l_{SL} \\ max\left(l_{LG}, l_{SL}\right) & \leq r_{min} \\ l_z & \leq \sup_{i=\overline{1,n-1}, k=\overline{1,N_i}} z_i \end{cases} \tag{7}$$

has a solution (for more details see[24,26,27,25], where

$$r_{min} = \inf_{i_k \in [i,i+1]} d\left(O_2, P_{i_k}\right), \quad r_{max} = \sup_{i_k \in [i,i+1]} d\left(O_2, P_{i_k}\right) \tag{8}$$

for any $i = \overline{1, n-1}$.

3 | END-EFFECTOR PATH PLANNING

The path can be parameterized[22,24,25] using the cylindrical coordinate r, θ and z by $\mathbf{r} = r(\theta)\cos\theta\mathbf{i}_0 + r(\theta)\sin\theta\mathbf{j}_0 + z\mathbf{k}_0$, that is

$$\mathbf{r} = \begin{bmatrix} r\cos\theta \\ r\sin\theta \\ z \end{bmatrix} = \begin{bmatrix} \sum_{k=0}^{3} c_k^i \left(\theta - \theta_i\right)^k \cos\theta \\ \sum_{k=0}^{3} c_k^i \left(\theta - \theta_i\right)^k \cos\theta \\ \sum_{k=0}^{3} C_k^i \left(x - x_i\right)^k \end{bmatrix} \tag{9}$$

The unit vectors $\mathbf{i}_0$, $\mathbf{j}_0$, $\mathbf{k}_0$ can be expressed in a Frenet frame by $\mathbf{i}_0 = \cos\theta\mathbf{e}_r - \sin\theta\mathbf{e}_\theta$, $\mathbf{j}_0 = \sin\theta\mathbf{e}_r + \cos\theta\mathbf{e}_\theta$, $\mathbf{k}_0 = \mathbf{e}_z$. The velocity vector $\mathbf{v} = \dot{\mathbf{r}} = \dot{r}\mathbf{e}_r + r\dot{\theta}\mathbf{e}_\theta + \dot{z}\mathbf{e}_z$ is written with

$$\mathbf{v} = \begin{bmatrix} \dot{\theta}\sum_{k=0}^{3} c_k^i k \left(\theta - \theta_i\right)^{k-1} \cos\theta - \dot{\theta}\sum_{k=0}^{3} c_k^i \left(\theta - \theta_i\right)^k \sin\theta \\ \dot{\theta}\sum_{k=0}^{3} c_k^i k \left(\theta - \theta_i\right)^{k-1} \cos\theta + \dot{\theta}\sum_{k=0}^{3} c_k^i \left(\theta - \theta_i\right)^k \cos\theta \\ \dot{x}\sum_{k=0}^{3} C_k^i k \left(x - x_i\right)^{k-1} \end{bmatrix} \tag{10}$$

where the derivative of $r = r(\theta)$ was calculated using $\dot{r}(\theta) = \dot{\theta}\sum_{k=0}^{3} c_k^i k \left(\theta - \theta_i\right)^{k-1}$, and the derivative of $z = z(x)$ was calculated using $\dot{z}(x) = \dot{x}\sum_{k=0}^{3} C_k^i k \left(x - x_i\right)^{k-1}$. It results

$$v = \sqrt{\begin{array}{l} \left(\dot{\theta}\sum_{k=0}^{3} c_k^i k \left(\theta - \theta_i\right)^{k-1} \cos\theta - \dot{\theta}\sum_{k=0}^{3} c_k^i \left(\theta - \theta_i\right)^k \sin\theta\right)^2 \\ +\left(\dot{\theta}\sum_{k=0}^{3} c_k^i k \left(\theta - \theta_i\right)^{k-1} \cos\theta + \dot{\theta}\sum_{k=0}^{3} c_k^i \left(\theta - \theta_i\right)^k \cos\theta\right)^2 \\ +\left(\dot{x}\sum_{k=0}^{3} C_k^i k \left(x - x_i\right)^{k-1}\right)^2 \end{array}} \tag{11}$$

The acceleration vector can be written as $\mathbf{a} = \dot{\mathbf{v}} = \ddot{\mathbf{r}} = \left(\ddot{r} - r\dot{\theta}^2\right)\mathbf{e}_r + \left(2\dot{r}\dot{\theta} - r\ddot{\theta}^2\right)\mathbf{e}_\theta + \ddot{z}\mathbf{e}_z$ by

$$
\begin{aligned}
\mathbf{a} &= \begin{bmatrix}
\left(\ddot{r} - \dot{\theta}^2 \sum_{k=0}^{3} c_k^i \left(\theta - \theta_i\right)^k\right)\cos\theta - \left(\ddot{\theta}\sum_{k=0}^{3} c_k^i\left(\theta-\theta_i\right)^k + 2\dot{r}\dot{\theta}\right)\sin\theta \\
\left(\ddot{r} - \dot{\theta}^2 \sum_{k=0}^{3} c_k^i \left(\theta - \theta_i\right)^k\right)\sin\theta - \left(\ddot{\theta}\sum_{k=0}^{3} c_k^i\left(\theta-\theta_i\right)^k + 2\dot{r}\dot{\theta}\right)\cos\theta \\
\ddot{x}\sum_{k=1}^{3} C_k^i k\left(x - x_i\right)^{k-1} + \dot{x}^2\sum_{k=2}^{3} C_k^i (k-1)k\left(x - x_i\right)^{k-2}
\end{bmatrix} \\
&= \begin{bmatrix}
\left(-\dot{\theta}^2\sum_{k=0}^{3} c_k^i\left(\theta-\theta_i\right)^k + \ddot{\theta}\sum_{k=1}^{3} c_k^i k\left(\theta-\theta_i\right)^{k-1} + \dot{\theta}^2\sum_{k=2}^{3} c_k^i (k-1)k\left(\theta-\theta_i\right)^{k-2}\right)\cos\theta \\
\left(-\dot{\theta}^2\sum_{k=0}^{3} c_k^i\left(\theta-\theta_i\right)^k + \ddot{\theta}\sum_{k=1}^{3} c_k^i k\left(\theta-\theta_i\right)^{k-1} + \dot{\theta}^2\sum_{k=2}^{3} c_k^i (k-1)k\left(\theta-\theta_i\right)^{k-2}\right)\sin\theta \\
\ddot{x}\sum_{k=1}^{3} C_k^i k\left(x - x_i\right)^{k-1}
\end{bmatrix} \\
&+ \begin{bmatrix}
\left(-\ddot{\theta}\sum_{k=0}^{3} c_k^i\left(\theta-\theta_i\right)^k - 2\dot{\theta}^2\sum_{k=1}^{3} c_k^i k\left(\theta-\theta_i\right)^{k-1}\right)\sin\theta \\
\left(\ddot{\theta}\sum_{k=0}^{3} c_k^i\left(\theta-\theta_i\right)^k + 2\dot{\theta}^2\sum_{k=1}^{3} c_k^i k\left(\theta-\theta_i\right)^{k-1}\right)\cos\theta \\
\dot{x}^2\sum_{k=2}^{3} C_k^i (k-1)k\left(x-x_i\right)^{k-2}
\end{bmatrix}
\end{aligned}
\tag{12}
$$

where $\ddot{r}(\theta) = \ddot{\theta}\sum_{k=1}^{3} c_k^i k\left(\theta-\theta_i\right)^{k-1} + \dot{\theta}^2\sum_{k=2}^{3} c_k^i (k-1)k\left(\theta-\theta_i\right)^{k-2}$, and the second derivative of z was calculated using $\ddot{z} = \ddot{x}\sum_{k=1}^{3} C_k^i k\left(x-x_i\right)^{k-1} + \dot{x}^2\sum_{k=2}^{3} C_k^i (k-1)k\left(x-x_i\right)^{k-2}$.

4 | KINEMATICS

The generalised coordinates θ_{C_1}, z_{C_2} and r_{C_3} (Fig. 2) relates to the centre of the mass of link 0 (z-guide zG), link 1 (the rigid sliding guide RG), and respectively link 2 (sliding hand support SL). The frames $O_0x_0y_0z_0$ and $O_1x_1y_1z_1$ are defined by $\mathbf{i}_0 = \mathbf{i}, \mathbf{j}_0 = \mathbf{j}, \mathbf{k}_0 = \mathbf{k}$, and respectively by $\mathbf{i}_1, \mathbf{j}_1, \mathbf{k}_1$ (Fig. 3). The Euler angles[28] relates $\mathbf{i}_1, \mathbf{j}_1, \mathbf{k}_1$ and $\mathbf{i}_0, \mathbf{j}_0, \mathbf{k}_0$ by

$$
\begin{bmatrix} \mathbf{i}_1 \\ \mathbf{j}_1 \\ \mathbf{k}_1 \end{bmatrix} = \begin{bmatrix} \cos\theta & -\sin\theta & 0 \\ \sin\theta & \cos\theta & 0 \\ 0 & 0 & 1 \end{bmatrix} \begin{bmatrix} \mathbf{i}_0 \\ \mathbf{j}_0 \\ \mathbf{k}_0 \end{bmatrix}
\tag{13}
$$

No other reference frames are needed since the mobile reference frame defined by $\mathbf{i}_1, \mathbf{j}_1, \mathbf{k}_1$ can be properly used to express all the link's position, velocity (respectively angular velocity) and acceleration (respectively angular acceleration). The angular velocity/acceleration of link 1, 2 and 3 can be expressed by

$$
\begin{aligned}
\boldsymbol{\omega}_1 &= \boldsymbol{\omega}_2 = \boldsymbol{\omega}_3 = \dot{\theta}\mathbf{k}_1 = \dot{\theta}\mathbf{k}_0 \\
\boldsymbol{\alpha}_1 &= \boldsymbol{\alpha}_2 = \boldsymbol{\alpha}_3 = \ddot{\theta}\mathbf{k}_1 = \ddot{\theta}\mathbf{k}_0
\end{aligned}
\tag{14}
$$

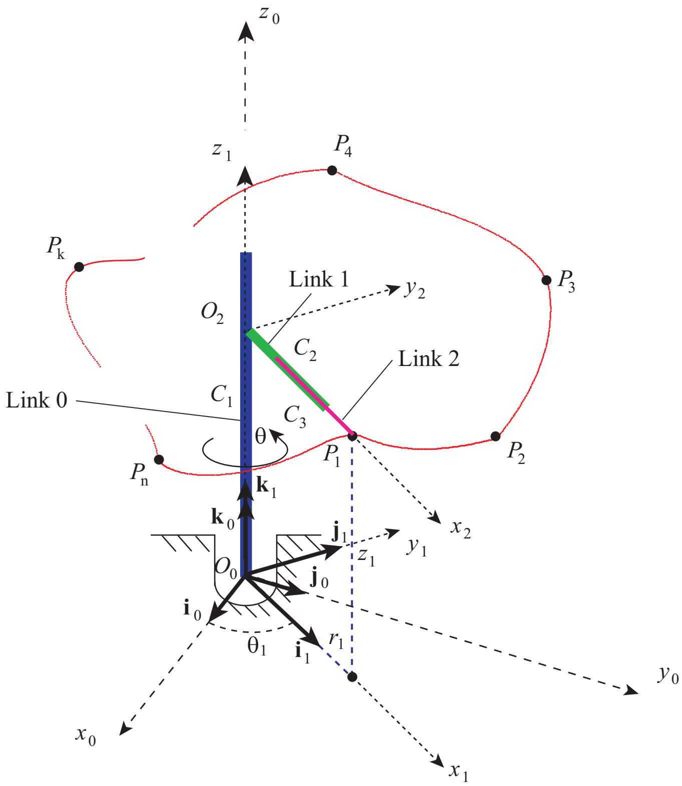

FIGURE 2 Reference frames and robotic arm model

The position of the mass center of link 1, link 2 and link 3, can be calculated wirh

$$\begin{aligned}
\mathbf{r}_{C_1} &= \frac{l_{zG}}{2}\mathbf{k}_1 = \frac{l_{zG}}{2}\mathbf{k}_0 \\
\mathbf{r}_{C_2} &= z_{C_2}\mathbf{k}_1 + \frac{l_{RG}}{2}\mathbf{j}_1 \\
&= \frac{l_{RG}}{2}\sin\theta\mathbf{i}_0 + \frac{l_{RG}}{2}\cos\theta\mathbf{j}_0 + z_{C_2}\mathbf{k}_0 \\
\mathbf{r}_{C_3} &= z_{C_2}\mathbf{k}_1 + r_{C_3}\mathbf{j}_1 \\
&= r_{C_3}\sin\theta\mathbf{i}_0 + r_{C_3}\cos\theta\mathbf{j}_0 + z_{C_2}\mathbf{k}_0
\end{aligned} \tag{15}$$

The velocity of the mass center of link 1, link 2 and link 3 can be calculate with

$$\begin{aligned}
\mathbf{v}_{C_1} &= \frac{d}{dt}\mathbf{r}_{C_1} = \dot{\mathbf{r}}_{C_1} = \mathbf{0} \\
\mathbf{v}_{C_2} &= \frac{d}{dt}\mathbf{r}_{C_2} = \frac{d}{dt}\left(\frac{l_{RG}}{2}\sin\theta\mathbf{i}_0 + \frac{l_{RG}}{2}\cos\theta\mathbf{j}_0 + z_{C_2}\mathbf{k}_0\right) \\
&= \frac{1}{2}l_{RG}\dot{\theta}\cos\theta\mathbf{i}_0 - \frac{1}{2}l_{RG}\dot{\theta}\sin\theta\mathbf{j}_0 + \dot{z}_{C_2}\mathbf{k}_0 \\
\mathbf{v}_{C_3} &= \frac{d}{dt}\mathbf{r}_{C_3} = \frac{d}{dt}\left(r_{C_3}\sin\theta\mathbf{i}_0 + r_{C_3}\cos\theta\mathbf{j}_0 + z_{C_2}\mathbf{k}_0\right) \\
&= \cos\theta\left(\dot{l}_{C_3}\tan\theta + r_{C_3}\dot{\theta}\right)\mathbf{i}_0 + \cos\theta\left(\dot{l}_{C_3} - r_{C_3}\dot{\theta}\tan\theta\right)\mathbf{j}_0 + \dot{z}_{C_2}\mathbf{k}_0
\end{aligned} \tag{16}$$

The acceleration the mass center of link 1, link 2 and link 3 can be calculate with

$$
\begin{aligned}
\mathbf{a}_{C_1} &= \frac{d}{dt}\mathbf{v}_{C_1} = \ddot{\mathbf{r}}_{C_1} = \mathbf{0} \\
\mathbf{a}_{C_2} &= \frac{d}{dt}\mathbf{v}_{C_2} = \frac{d}{dt}\left(\frac{1}{2}l_{RG}\dot{\theta}\cos\theta\mathbf{i}_0 - \frac{1}{2}l_{RG}\dot{\theta}\sin\theta\mathbf{j}_0 + \dot{z}_{C_2}\mathbf{k}_0\right) \\
&= \frac{1}{2}l_{RG}\cos\theta\left(\ddot{\theta} - \dot{\theta}^2\tan\theta\right)\mathbf{i}_0 - \frac{1}{2}l_{RG}\cos\theta\left(\ddot{\theta}\tan\theta + \dot{\theta}^2\right)\mathbf{j}_0 + \ddot{z}_{C_2}\mathbf{k}_0 \\
\mathbf{a}_{C_3} &= \frac{d}{dt}\mathbf{v}_{C_3} \\
&= \frac{d}{dt}\left\{\left(\dot{l}_{C_3}\sin\theta + r_{C_3}\dot{\theta}\cos\theta\right)\mathbf{i}_0 + \left(\dot{l}_{C_3}\cos\theta - r_{C_3}\dot{\theta}\sin\theta\right)\mathbf{j}_0 + \dot{z}_{C_2}\mathbf{k}_0\right\} \\
&= \cos\theta\left(\ddot{l}_{C_3}\tan\theta + 2\dot{l}_{C_3}\dot{\theta} + r_{C_3}\ddot{\theta} - r_{C_3}\dot{\theta}^2\tan\theta\right)\mathbf{i}_0 \\
&\quad + \cos\theta\left(\ddot{l}_{C_3} - 2\dot{l}_{C_3}\dot{\theta}\tan\theta - r_{C_3}\ddot{\theta}\tan\theta - r_{C_3}\dot{\theta}^2\right)\mathbf{j}_0 + \ddot{z}_{C_2}\mathbf{k}_0
\end{aligned}
\tag{17}
$$

5 | RESULTS

Two numerical examples[28,29] are presented to illustrate trajectory generation of a z-guide of maximal height $l_z = 1.2$ m, rigid guide with $l_G = 0.55$ m and a sliding link with $l_{SL} = 0.55$ m. The trajectory generation in which the end-effector moves smoothly[27] mix match polar and Cartesian piecewise polynomials. The numerical values of the via-points coordinates are presented in Table 1.

TABLE 1 Via-points for the 1-st configuration of the robotic arm

Parameter	Parameter Value								
i	1	2	3	4	5	6	7	8	9=1
θ_i	20	50	130	150	210	270	310	350	360+20
r_i	12	9	2	10	10	5	7	10	12
z_i	7	12	3	14	5	9	7	10	7

Path planning for the configuration in Table 1, obtained by mix matching polar and Cartesian piecewise interpolating curves is shown in Fig. 3. Figures 3a, 3c and 3b represents the projection of end-effector trajectory on the $O_0x_0y_0$ (radial trajectory of the end-effector), $O_0x_0z_0$ and $O_0y_0z_0$ plane respectively. For this simulation, although a working trajectory is obtained, it can be seen that the robotic end effector is in the proximity but still outside the working envelope, that is, it cannot handle all the desired via-points shown in Table 1 when following the computed path (Fig. 3a).

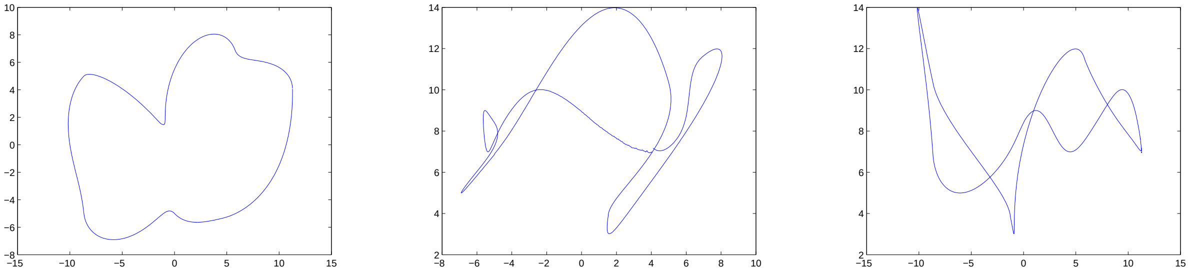

(a) Oxy plane **(b)** Oxz plane **(c)** Oyz plane

FIGURE 3 End-effector trajectory generated using Hermite polar and Cartesian interpolation

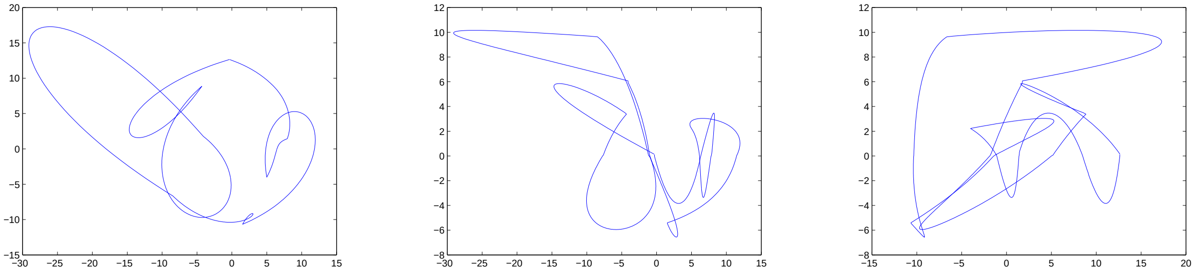

(a) Oxy plane **(b)** Oxz plane **(c)** Oyz plane

FIGURE 4 End-effector velocity curves

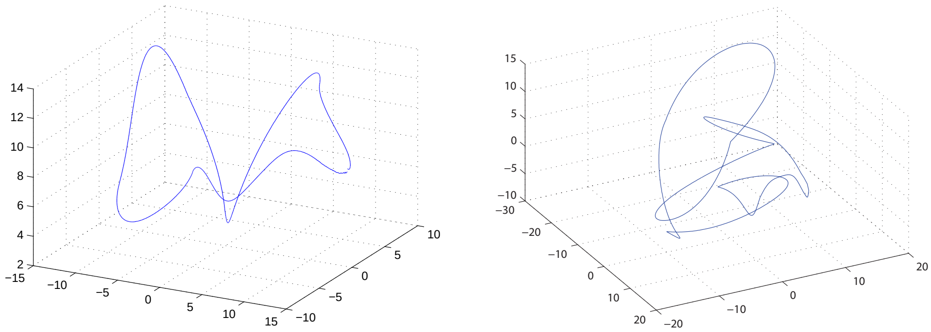

(a) End-effector position **(b)** End-effector velocity

FIGURE 5 3D trajectory position and velocity of the end-effector

The velocity projection on the $O_0x_0y_0$, $O_0x_0z_0$ and $O_0y_0z_0$ planes denoted by v_{xy}, v_{xz}, and v_{yz} are shown in Fig. 4a, Fig. 4b and respectively in Fig. 4c.

To better understand the system behaviour, the trajectory (position and velocity) of the robotic arm is shown in the 3 dimensional space in Fig. 5a and Fig. 5b. The smoothness of the continuous position and velocity curves shown in Fig. 5 prove the effectiveness of the trajectory planning of the end-effector of the 3D mechanism. As a result, the forces needed to guide arm of the robot along the prescribed path, are also continuous. A second numerical example with the associated data shown in Table 2 is then considered. For this second configuration Eq. 7 is verified, that is, the robotic arm is placed inside the working envelope thus all the via-points in Table 2 and shown in Fig. 7 can be reached.

TABLE 2 Via-points for the 2-nd configuration of the robotic arm

Parameter	Parameter Value								
i	1	2	3	4	5	6	7	8	9=1
θ_i	45	90	135	180	225	270	315	360	360+45
r_i	10	6	11	7	10	6	11	7	10
z_i	6	11	7	12	8	13	9	14	6

The end-effector trajectories of the robotic arm representing the projections on the $O_0x_0y_0$ (radial trajectory of the end-effector), $O_0x_0z_0$ and $O_0y_0z_0$ plane are shown Fig. 6a, Fig. 6b and Fig. 6c. The end-effector trajectory position and velocity of the robotic arm is shown in the 3 dimensional space in Fig. 7a and Fig. 7b. The smoothness of the continuous position and velocity proves again the performance of the method. Therefore, the forces acting on the end-effector of the robotic arm along the generated path are also continuous.

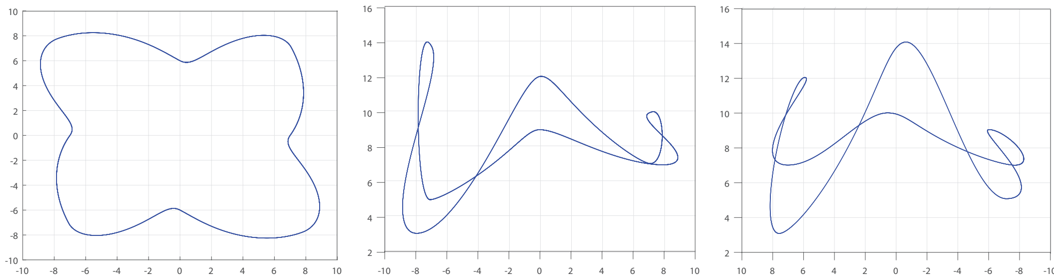

(a) Oxy plane **(b)** Oxz plane **(c)** Oyz plane

FIGURE 6 End-effector trajectory projections

6 | CONCLUSION

In this study the modelling and simulation of a robotic arm and the associated 3D trajectory planning of its end-effector is presented. The robotic arm trajectory – expressed in cylindrical coordinates – is generated using a mix matched polar and Cartesian piecewise Hermite–type polynomials in order to approximate the radial path and associated height respectively. Due to the system geometry which constrains the trajectory inside the working envelope, the existence of a solution in relation with the base of the robotic arm is addressed. Two numerical simulations are performed for two different configurations to validate the solution in relation with the working envelope.

References

1. A. Gasparetto AL, Vidoni R. Trajectory planning in robotics. *Mathematics in Computer Science* 2012; 6: 269–279.
2. D. Hsu JL, Rock S. Randomized kinodynamic motion planning with moving obstacles. *International Journal of Robotics Research* 2002; 21(3): 233–255.
3. Dupac M. Kinematics and dynamics motion planning by polar piecewise interpolation and geometric considerations.. *Electronic Notes in Discrete Mathematics* 2018; 67: 19–24.

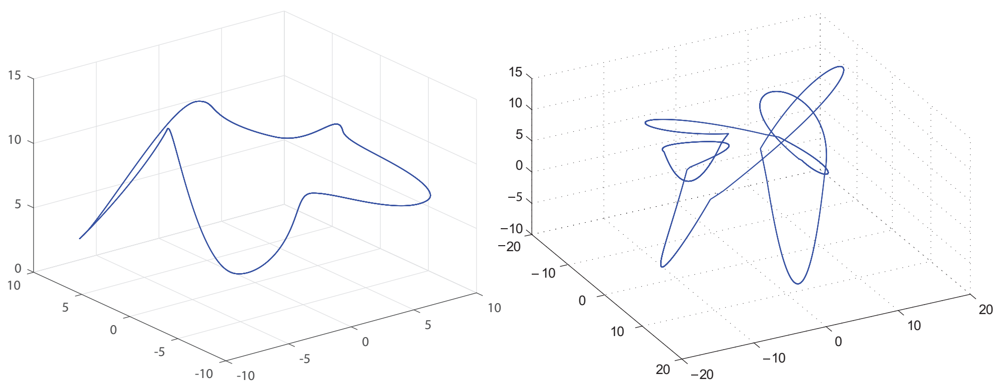

(a) End-effector position **(b)** End-effector velocity

FIGURE 7 3D end-effector trajectory position and velocity of the robotic arm

4. J.E. Bobrow SD, Gibson J. Time-optimal control of robotic manipulators along specified paths. *International Journal of Robotics Research* 1985; 4(3): 3–17.

5. J. Dong PF, Stori J. Feed-rate optimization with jerk constraints for generating minimum-time trajectories. *International Journal of Machine Tools and Manufacture* 2007; 47(12): 1941–1955.

6. Lo H, Xie S. Exoskeleton robots for upper–limb rehabilitation: State of the art and future prospects. *Medical Engineering and Physics* 2012; 34: 261–268.

7. P.R. Culmer SMJCMLMMW, Bhakta B. A novel robotic system for quantifying arm kinematics and kinetics: Description and evaluation in therapist-assisted passive arm movements post-stroke. *Journal of Neuroscience Methods* 2011; 197: 259–269.

8. Q. Miao MZPK, Li H. A three-stage trajectory generation method for robot-assisted bilateral upper limb training with subject-specific adaptation. *Robotics and Autonomous Systems* 2018; 105: 38–46.

9. B. Brahmi JLCLPA, Rahman M. Adaptive control of a 7-DOF exoskeleton robot with uncertainties on kinematics and dynamics. *Journal of Neuroscience Methods* 2018; 42: 77–87.

10. J.C. Fraile EBPVRAACMFMEPLAFGBFNLL. E2Rebot: A robotic platform for upper limb rehabilitation in patients with neuromotor disability. *Advances in Mechanical Engineering* 2016; 8(8): 1–13.

11. K. Liu LHWBC, Huang XL. Postural synergy based design of exoskeleton robot replicating human arm reaching movements. *Robotics and Autonomous Systems* 2018; 99: 84–96.

12. A. Mancisidor ICPB, Jung JH. Kinematical and dynamical modeling of a multipurpose upper limbs rehabilitation robot. *Robotics and ComputerâĂŞIntegrated Manufacturing* 2018; 49: 374–387.

13. C.S. Lin PC, Luh J. Formulation and optimization of cubic polynomial joint trajectories for industrial robots. *IEEE Transactions on Automatic Control* 1983; 28(12): 1066–1073.

14. Sanchez-Reyes J. Single-valued spline curves in polar coordinates. *Computer Aided Design* 1992; 24: 307–315.

15. Goodman T, Lee S. B-splines on the circle and trigonometric B-splines. *Approximation Theory and Spline Functions* 1984; 136: 297–325.

16. Kang I, Park F. Cubic spline algorithms for orientation interpolation. *International Journal for Numerical Methods in Engineering* 1999; 46: 45–64.

17. Adhami L, Coste E. Optimal planning for minimally invasive surgical robots. *IEEE Transactions on Robotics and Automation* 2003; 19(5): 854–863.

18. Plessis dL, Snyman J. Trajectory-planning through interpolation by overlapping cubic arcs and cubic splines. *International Journal for Numerical Methods in Engineering* 2003; 57: 1615–1641.

19. Su B, Zou L. Manipulator trajectory planning based on the algebraic trigonometric Hermite blended interpolation spline. *Procedia Engineering* 2012; 29: 2093–2097.

20. Kalyoncu M. Mathematical modelling and dynamic response of a multistraight-line path tracing flexible robot manipulator with rotating-prismatic joint. *Procedia Engineering* 2008; 32: 1087–1098.

21. Dupac M. A virtual prototype of a constrained extensible crank mechanism: dynamic simulation and design. *Proceedings of the Institution of Mechanical Engineers, Part K: Journal of Multi-body Dynamics* 2013; 227(3): 201–210.

22. Dupac M. A path planning approach of 3D manipulators using zenithal gnomic projection and polar piecewise interpolation. *Mathematical Methods in Applied Sciences*. doi: 10.1002/mma.4790

23. Iwashita Y. Piecewise polynomial interpolation. *Open Gamma Quantitative Research* 2014; 15: 1–22.

24. Dupac M, Sewell P. Quick 3D trajectory planning for rotating extensible manipulators using piecewise polynomial interpolation. *Proceedings of the Congress on Numerical Methods in Engineering, CMN 2017, 3–5 July, Valencia, Spain* 2017: 27–32.

25. Dupac M. Smooth trajectory generation for rotating extensible manipulators. *Mathematical Methods in Applied Sciences* 2018; 41(6): 2281–2286.

26. Kohli D, Spanos J. Workspace analysis of mechanical manipulators using polynomial discriminants. *Journal of Mechanisms, Transmissions, and Automation* 1985; 107(2): 209–215.

27. Y. Cao XL, Zang Y. Accurate numerical methods for computing 2D and 3D robot workspace. *International Journal of Advanced Robotic Systems* 2011; 8(6): 1–13.

28. Marghitu D, Dupac M. Advanced dynamics: analytical and numerical calculations with Matlab. *Springer, New-York* 2012.

29. Zlajpah L. Simulation in robotics. *Mathematics and Computers in Simulation* 2008; 79(4): 879–897.

□